International Atomic Energy Agency

INDC(CUB)-002
Distr.: L

INDC INTERNATIONAL NUCLEAR DATA COMMITTEE

ANALYSIS OF THE LOW ENERGY NEUTRON INELASTIC SCATTERING IN MASS RANGE $48 \leq A \leq 64$.

R. Cabezas, J. Lubian, J. Tomas
Institute for Nuclear Science and Technology
Havana, Cuba

April 1990

IAEA NUCLEAR DATA SECTION, WAGRAMERSTRASSE 5, A-1400 VIENNA

INDC(CUB)-002
Distr.: L

ANALYSIS OF THE LOW ENERGY NEUTRON INELASTIC SCATTERING IN MASS RANGE $48 \leq A \leq 64$.

R. Cabezas, J. Lubian, J. Tomas
Institute for Nuclear Science and Technology
Havana, Cuba

April 1990

Reproduced by the IAEA in Austria
April 1990

90-01542

ANALYSIS OF THE LOW ENERGY NEUTRON INELASTIC SCATTERING IN MASS RANGE 48 ≤ A ≤ 64.

R. Cabezas, J. Lubian, J. Tomas
Institute for Nuclear Science and Technology
Havana, Cuba

ABSTRACT

An analysis of low energy neutron inelastic scattering in medium-mass nuclei is made. A regional deformed optical model parameterization is proposed to describe the experimental data. This parameterization is derived from titanium, chromium, iron and nickel isotopes in the energy region of 1-3 MeV. A combined use of the coupled channel method and the statistical Hauser-Feshbach theory including corrections due to the presence of direct processes is applied. It is shown that, in the frame of this parameterization, it is possible to describe adequately experimental angular distributions, integral and total cross sections. An extrapolation to the energy region higher than 3 MeV is made. It is also shown, that this parameterization can be extended to other neighbour nuclei like zinc isotopes $^{64,66,68}Zn$.

INTRODUCTION

In the calculation and estimation of nuclear data for Fe, Ti, Ni and Cr isotopes - important structural materials in nuclear technology - the study of the neutron inelastic scattering at energies from 1 to 3 MeV plays a significant role. In this sense, a systematic study of optical potential parameters represents a great interest in order to obtain an adequate regional parameterization to describe the experimental data.

Up to now, it doesn't exist any parameterization of the optical potential, which allows us to describe experimental angular distributions and total cross-sections at low energies in the region of medium-mass nuclei 48≤A≤64 consistently [1,2]. For these nuclei, it's not possible to extrapolate the optical parameters for high energies to energies below 3 MeV [3].

In the inelastic scattering of low-energy neutrons, when contributions of direct and compound nucleus processes to the total cross-section are similar, calculations are usually carried out by adding the direct cross-section, calculated by means of the

coupled-channel method with deformed potentials, to the compound nucleus cross-section, calculated in the frame of the statistical theory of nuclear reactions with spherical optical model potential [4-6]. Nevertheless this consideration notably simplifies the calculation and in some cases becomes a good approximation, thus possibly leading us to physical ambiguities. Although the direct and compound nucleus processes are described by means of different formalisms, the nuclear potential should be the same.

On the other hand, there are some physical features that can influence on the description of experimental data in low-energy neutron calculations, for example:

i. In the 1-3 MeV energy region, collective modes in mass-medium nuclei are excited. For this reason, parameterizations based on the spherical optical potential are no longer a good approximation.

ii. In this energy region a few low-lying states are excited, so that the corrections to the compound nucleus cross-section can play a significant role.

iii. When the incident energy is comparable to the energies of the excited states, the coupling between elastic and inelastic channels is stronger, producing changes in the real potential similar to the observed Fermi potential anomaly [7,8].

Compound nucleus cross-section calculations considering the weak coupling between channels in the weak absorption case were formulated by Engelbrecht and Weidenmüller [9]. A more general case was treated by Hofmann *et al* [10] and independently by Moldauer [11]. In these works it was shown, that in the presence of direct processes the compound nucleus cross-section may be calculated by means of the Hauser-Feshbach formalism with transmission coefficients that take into account the presence of direct transitions.

In the present work, starting from the analysis of experimental angular distributions, integral and total cross-sections reported in the EXFOR library for nuclei ^{48}Ti, ^{58,60,62,64}Ni, ^{54,56}Fe, ^{50,52,54}Cr , a regional parameterization of the optical potential based on the combined use of the coupled-channel and theHauser-Feshbach methods is proposed. The inclusion of direct process effects in the calculation of compound nucleus cross-sections was considered by mean of the consistent combination of both methods, using Satchler generalized transmission coefficients [12].

DETERMINATION OF THE REGIONAL OPTICAL MODEL PARAMETERIZATION FOR COUPLED CHANNEL CALCULATION.

The optical potential was taken in its conventional form [13], consisting in a real part with the Woods-Saxon form-factor, a surface imaginary part with derivative of the Woods-Saxon form-factor and a real spin-orbital Thomas term. It has the following form:

$$V(r) = U\, f_u(r) - 4ia_v W_s \frac{df_v(r)}{dr} + \left(\frac{\hbar^2}{m_\pi c}\right)^2 \frac{1}{r} U_{so} \frac{df_{so}(r)}{dr} (\hat{L}\cdot\hat{\sigma}) \qquad (1)$$

where U, W_s and U_{so} are the depths of real, surface imaginary and spin-orbital potentials, respectively;

$$f_i(r) = [1+\exp\{(r-R_i)/a_i\}]^{-1}$$

is the Woods-Saxon form-factor; a_i and $R_i = r_i A^{1/3}$ are the diffusenesses and radii of the corresponding potentials.

The parameterization of the spherical optical potential obtained by Pasechnik *et al.* [14] for medium-mass nuclei in the energy region up to 10 MeV was taken as a starting point for the analysis. It is expressed as follows:

$$\begin{aligned} &U = (48.7 - 0.33E)\ \text{MeV} && r_v = r_v = r_{so} = 1.25\ \text{f} \\ &W_s = (7.2 + 0.66E)\ \text{MeV} && a_v = a_{so} = 0.65\ \text{f} \\ &U_{so} = 7.5\ \text{MeV} && a_v = 0.43\ \text{f} \end{aligned} \qquad (2)$$

The wave function of the harmonic vibrator considering one-phonon and two-phonon excitations was taken as a basis wave function in the coupled channel equation. In this sense, the expansion of the nuclear radius in spherical harmonics was considered up to the quadrupolar term:

$$R_i = r_i \left[\, 1 + \beta_2 Y_{20} \,\right] \qquad (3)$$

Parameters β_2 for different isotopes were taken from Ref. 15, considering the normalization to the radius r_i used in this work.

The fitting procedure of parameters was made in the following way: initially, the experimental angular distributions separately for four energy values (1.5; 2.0; 2.5; 3.0 MeV) for each isotope were fitted. For this purpose, the χ^2 procedure implemented in the ECIS87 code [16] was used minimizing the quantity:

$$\chi^2 = \frac{1}{N} \sum_{i=1}^{N} \left[\frac{\sigma_{exp}(\theta_i) - \sigma_{calc}(\theta_i)}{\Delta\sigma_{exp}(\theta_i)} \right]^2 \qquad (4)$$

where $\sigma_{exp}(\theta_i)$ is the measured value at angle θ_i, $\Delta\sigma_{exp}(\theta_i)$ its

uncertainty, $\sigma_{calc}(\theta_i)$ the corresponding calculated value, and N is the number of data points contained in a given distribution.

For choosing the coupling scheme, the following criterion was followed:

1-To consider the same number of coupled channels for all nuclei in the whole energy range. This condition is essential for a correct derivation of surface imaginary parameters due to its sensibility to the number of coupled channels.

2-To assume as coupled all the channels that are opened up to 3 MeV in all studied nuclei. It means to take into account six coupled channels.

3-To include as uncoupled channels all known levels above 3 MeV reported in literature (see Ref.17). The influence of the closed channels plays an important role in the correct description of experimental data. Including these channels, it is possible to consider implicitly the contribution of the intermediate structure [18].

For each assumed energy, the minimization of the deformed optical potential parameters was carried out trying to satisfy the inequality:

$$\chi^2/N \leq 10. \qquad (5)$$

The result of the variation shows that geometrical parameters and depth V_{so} vary very slowly with energy and from one isotope to another. For this reason, the mean value of these parameters was assumed for all nuclei:

$$\begin{aligned} a_v &= a_{so} = 0.645 \text{ f} \\ r_v &= r_w = r_{so} = 1.244 \text{ f} \\ a_w &= 0.434 \text{ f} \\ V_{so} &= 7.418 \text{ MeV} \end{aligned} \qquad (6)$$

As soon as elastic and inelastic angular distributions for each nucleus were fitted, we began the search of the regional parameters U and W as a function of the incident energy E and the isotopic factor $\eta=(N-Z)/A$.The result of the calculations (explained in details in Ref.19) shows that the best fit is obtained for the following expressions:

$$U = 52.095 - 0.735E - 0.195E^2 - 11.528\cdot[1-0.171E]\eta \ , \qquad (7)$$

$$W_s = 0.343 - 0.337E + 0.304E^2 - 1.234\cdot[1-1.366E]\eta \ . \qquad (8)$$

It is important to emphasize that the linear dependence on the energy didn't fit well. The inclusion of the quadratic term was the best way to carry out a satisfactory fit for all nuclei. This non-linear dependence of real potential is in correspondence to the anomaly of the real potential near the Fermi surface observed in different papers [8,20].

The non-linear behavior of the real potential is equivalent to considerate an energy dependent real potential radius. Since we consider the real potential radius to be constant in our work, the non-linear dependence of the real potential is understandable.

Moreover, if we compare the non-linear and quadratic coefficients of our work with other global parameterizations using spherical optical potential obtained by other authors, it can be seen that our linear term coefficient is twice bigger than those shown in Ref.2, and the quadratic term coefficient is two-three times bigger than those ones. This deviation can be conditioned by the consideration of collective effects (one-phonon and two-phonon vibrations of these nuclei) and the strong coupling between the low-lying states, which at low energies play an important role.

The evaluation of W_s using eq.(8) for all studied nuclei in the energy interval 1-3 MeV provides that W_s varies from Ø.3 to 2.6 MeV. These values of surface imaginary potential are significantly smaller than those obtained by means of the spherical optical potential. This decrease was expected because the inelastic processes and part of the doorway states effect were implicitly considered in the calculations taking into account the coupling between many channels and the inclusion of many uncoupled states.

COMPARISON OF THE THEORETICAL RESULTS WITH EXPERIMENTS.

Using the expressions obtained for U and W_s in (7-8) and taking into account the mean values for the other parameters given in (6), calculations of angular distributions for ^{48}Ti, ^{58,60,62,64}Ni, ^{54,56}Fe, ^{50,52,54}Cr at energies 1.5; 2.Ø; 2.5; 3.Ø MeV (and 2.33; 2.9 MeV, when experimental data were available) were carried out. Figures 1-22 show the results of some of these calculations. Experimental data were taken from the EXFOR library. It can be seen that the differential elastic cross-sections are in good agreement with most of the isotopes studied in our work. For the inelastic differential cross-sections, a little increase of

the theoretical results is observed in a great number of them, particularly, in one-phonon states 2_1^+.

Figs. 23-38 show integral and total cross-sections for some studied isotopes and their comparison to experimental and evaluated data. If we compare the results of our calculation (full line) with the evaluated data from BROND (dashed line) library and experimental data from different authors, we can see that the agreement is good. The fine structure observed in our case, mainly at energies below 2 MeV, could be caused by the implicit consideration of the intermediate structure through the coupling between many channels. A more complete set of theoretical calculations related to this work can be found in Ref.19.

These results could be improved. In our analysis, to describe the structure of all isotopes, the second order harmonic vibrational model was assumed. In the frame of this model, collective excitations are considered purely one-phonon and two-phonon ones. In the same way, dynamical deformation parameters β_λ for all levels are taken with the same strength and equal to the quadrupolar one β_2.

Nevertheless, it is known, that different nuclei in this mass region show a deviation from the harmonic oscillations [21-23], manifesting evidences of anharmonic vibrations [24], nonaxiality [25] and so on. Considerations of this structural features in the coupled channel methods could improve obtained results. This analysis is in progress.

EXTRAPOLATION TO THE ENERGY REGION ABOVE 3 MeV AND EXTENTION TO OTHER ISOTOPES.

As soon as a good description in the energy region 1-3 MeV was obtained, we analyzed the possibility of application of our parameterization outside this energy region. In Figs 23-38 results of calculation of integral and total cross-sections for energies up to 5 MeV are shown. It can be seen that a good agreement with experimental data is reached. It is important to emphasize that it was possible, using our parameterization, to describe excitation functions for collective modes higher than one-phonon state 2_1^+. These high states have a more complex nature and they haven't been described by mean of other parameterizations reported in literature.

In Figs 39-44 results of calculation of integral cross-sections for ^{64,66,68}Zn at energy region 1-3 MeV are shown. The agreement with experimental data is good.

The use of this parameterization allows us to study even-even nuclei in the mass number range 48-68, in the energy region 1-5 MeV, as harmonic vibrational model is a good approximation to describe the low-lying states of the spectrum.

CONCLUSIONS

Interesting results have been obtained in our research.

A deformed optical potential regional parameterization was deduced, considering strong coupling of many channels and the influence of direct processes in compound nucleus calculations using generalized transmission coefficients. The obtained parameterization describes experimental angular distributions, integral and total cross-sections for different even-even isotopes of Ti, Cr, Fe, Ni and Zn.

In order to improve obtained results we propose:

- To consider more realistically collective excitations including anharmonism, nonaxiality and other features of the nuclear shape that could be present in these nuclei.
- To study a possible description of neutron strength function below 1 MeV.

The authors are gratefully to Dr. V.P. Lunev and Dr. V.G. Pronyaev for useful discussions and recommendations related to our work.

LITERATURE

1. Konshin V.A. Workshop on Applied Nuclear Theory and Nuclear Model Calculations for Nuclear Technology Applications, SMR/284-4, 15 febr-18 march 1988, ICTP, Trieste.
2. Young P.G. Proc. of the Specialists' Meeting on the Use of the Optical Model for the calculation of Neutron Cross-Sections bellow 20 MeV, Paris, 1985, p.125.
3. Wilmore D., Hodgson P.E. J. Phys. G11 (1985) 1007.
4. Simakov S.P., *et al.* Yadernaya Fizika 37 (1983) 801.
5. Ivanova S.P., Tsejpek Ya. Yadernaya Fizika 30 (1979) 1270.
6. Ramstrom A. Conf. on Nuclera Data for Science and Technollogy, Antwerp, 1983, p.597.
7. Gyarmati B. *et al.* J. Phys. G7 (1981) L209.
8. Hodgson P.E. INDC(NDS)-214/LJ, Jan. 1989, p.49.
9. Engelbrecht C.A., Weidenmüller H.A. Phys. Rev. C8 (1973) 859.
10. Hofmann H.M. *et al.* Ann. Phys. 90 (1975) 403.
11. Moldauer P.A. Phys. Rev. C12 (1975) 744.

12. Satchler G. Phys. Lett. 7 (1963) 55.
13. Hodgson P.E. Nuclear Reaction and Nuclear Structure, Clarendon Press, Oxford, 1971.
14. Pasechnik M.V., *et al.* Proc. of the Conf. on Neutron Physics, Kiev, 1972, part 1, p.253.
15. Raman S., *et al.* Atomic Data & Nuclear Data Tables 36 (1987) 1
16. Raynal J. ECIS87 Code. Unpublished.
17. Table of Isotopes, Ed. by Lederer C.M. and Shirley V.S., Wiley Interscience, 1978.
18. Ignatyuk A.V., *et al.* Proc. of the Int. Conf. on Neutron Physics, Moscow, 1988, part 2, p.70.
19. Cabezas R., Lubian J., Tomas J. Progress Report to the IAEA Research Contract 5431/RB, Aug 1989.
20. Mahaux C., Sartor R. Phys. Rev. C36 (1987) 1777.
21. Frois B., *et al.* Phys. Lett. 122B (1983) 347.
22. Gus P.P., *et al.* Nucl. Phys. A438 (1985) 187.
23. Mellema S., Finlay R.W., Dietrich F.S. Phys. Rev. C33 (1986) 481.
24. Rebel H., *et al.* Z. Phys. 256 (1972) 258.
25. Konshin V.A. Proc. of the IAEA Consultants' Meeting on Nuclear Data for Structural Materials, INDC(NDS)-152/L, IAEA, 1984, p.135.
26. Korzh A.I., *et al.* Yadernaya Fizika, 43 (1986) 1083.
27. Korzh A.I. *et al.* Proc. of the 2nd. All-Union Soviet Conference on Nuclear Physics, Obninsk, 1974, part 3, p.56.
28. Korzh A.I. *et al.* Ukrainsky Fizichesky Zhurnal 22 (1977) 112.
29. Korzh A.I. *et al.* Ukrainsky Fizichesky Zhurnal 22 (1977) 87.
30. EXFOR12972.001.
31. Sokolov *et al.* Ukrainsky Fizichesky Zhurnal 18 (1973) 263.
32. Rodgers *et al.* COO Report 1573-33, 1967.
33. EXFOR12752.004.
34. EXFOR12752.006.
35. Voss *et al.* 4th. Conference on Nuclear Cross-section and Technology, Washington D.C., 1975.
36. Guenther *et al.* Ann. of Nuclear Energy 13 (1986) 601.
37. Mittler *et al.* Priv. Com. Jun. 1975 (EXFOR10519.002).
38. Ramstrom E.A. Report AE-503, 1975, Helsinki. (EXFOR20788.007).
39. Guenther *et al* Nuclear Physics A 307 (1978) 229. EXFOR10669.002.
40. Broder *et al.* Voprosy Atomnoi Nauky y Tejniky. Seriya: Yadernie konstanty. 10 (1972) 13. (EXFOR40199.009).
41. Korzh *et al.* 3rd All-Union Conf. on Neutron Physics, Kiev, 1975. 4 (1976) 220.

Figure Captions.

Figs.1-7: Elastic and inelastic angular distribution for chromium isotopes. The experimental data were taken from Ref.27.

Figs.8-16: Elastic and inelastic angular distribution for nickel isotopes. The experimental data were taken from Ref.28.

Figs.17-20: Elastic and inelastic angular distribution for iron isotopes. The experimental data were taken from Ref.29.

Figs.21-22: Elastic and inelastic angular distribution for ^{48}Ti. The experimental data were taken from Ref.26,29.

Fig.23: Total cross-section for ^{58}Ni. The experimental data were taken from Ref.30. The full curve shous the results of our calculation and the dashed one, the evaluated data from BROND library.

Fig.24: Integral elastic cross-section for ^{58}Ni. The experimental data were taken from: • - Ref.28; ■ - Ref.31; ▲ - Ref.32; ◆ - Ref.33. The full curve shous the results of our calculation and the dashed one, the evaluated data from BROND library.

Fig.25: Integral inelastic cross-section for ^{58}Ni. The experimental data were taken from: ▲ - Ref.28; • - Ref.34; ■ - Ref.32. The full curve shous the results of our calculation and the dashed one, the evaluated data from BROND library.

Figs.26-27: Integral inelastic cross-sections for ^{58}Ni. The experimental data were taken from Ref.34.

Fig.28: Total cross-section for ^{50}Cr. The full curve shous the results of our calculation and the dashed one, the evaluated data from BROND library.

Fig.29: Integral elastic cross-section for ^{50}Cr. The experimental data were taken from Ref.27 . The full curve shous the results of our calculation and the dashed one, the evaluated data from BROND library.

Fig.30: Integral inelastic cross-section for ^{50}Cr. The experimental data were taken from: ▲ - Ref.27; • - Ref.35. The full curve shous the results of our calculation and the dashed one, the evaluated data from BROND library.

Fig.31: Total cross-section for ^{54}Fe. The experimental data were taken from Ref.36. The full curve shous the results of our calculation and the dashed one, the evaluated data from BROND library.

Fig.32: Integral elastic cross-section for ^{54}Fe. The experimental data were taken from: • - Ref.29; ▲ - Ref.32. The full curve shous the results of our calculation and the dashed one, the evaluated data from BROND library.

Fig.33: Integral inelastic cross-section for ^{54}Fe. The experimental data were taken from: • - Ref.29; ■ - Ref.37; ◆ - Ref.36; ▲ - Ref.38. The full curve shous the results of our calculation and the dashed one, the evaluated data from BROND library.

Figs.34-35: Integral inelastic cross-sections for ^{54}Fe. The experimental data were taken from Ref.36.

Fig.36: Total cross-section for ^{48}Ti. The experimental data were taken from Ref.39. (Natural titanium normalized)

Fig.37: Integral elastic cross-sections for ^{48}Ti. The experimental data were taken from Ref.27.

Fig.38: Integral inelastic cross-sections for ^{48}Ti. The experimental data were taken from: ▲ - Ref.27; ◆ - Ref.40.

Figs.39-44: Integral elastic and inelastic cross-sections for zinc isotopes. The experimental data were taken from Ref.41.

Fig.1 CR-50, En=1.5 MeV, 0+ g.s.
EL.C-S[MB/SR]

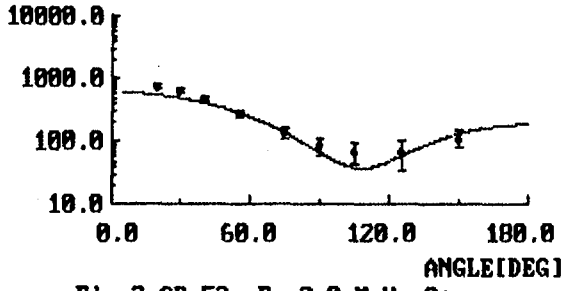

Fig.2 CR-50, En=1.5 MeV, 2+(0.783MeV)
INL.C-S[MB/SR]

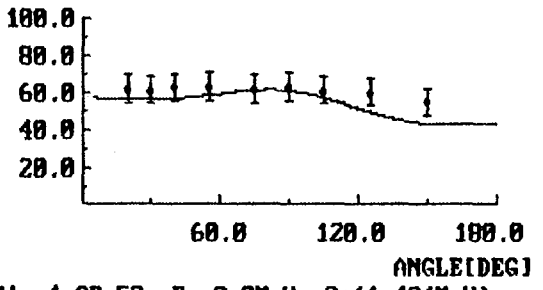

Fig.3 CR-52, En=3.0 MeV, 0+ g.s.
EL.C-S[MB/SR]

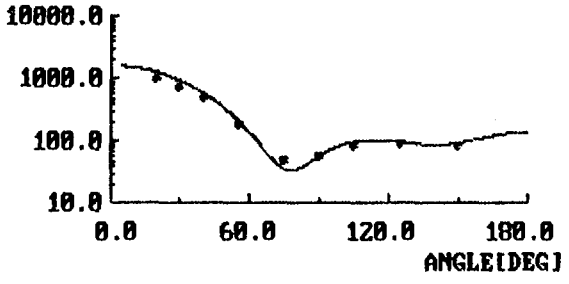

Fig.4 CR-52, En=3.0MeV, 2+(1.434MeV)
INL.C-S[MB/SR]

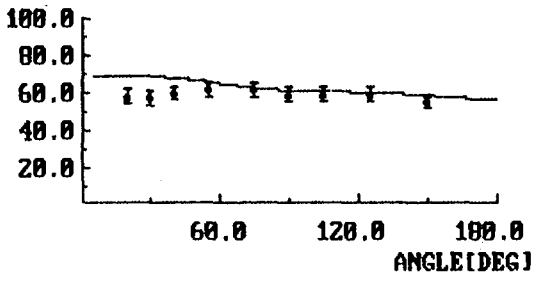

Fig.5 CR-52, En=3.0MeV, 4+(2.37MeV)
IN.C-S[MB/SR]

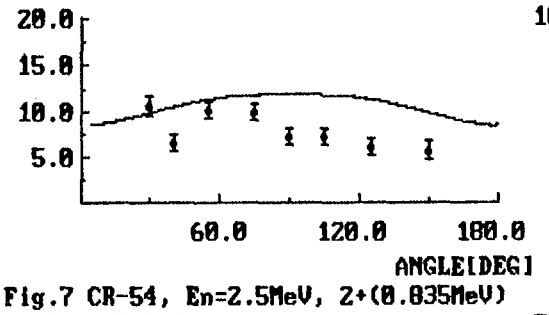

Fig.6 CR-54, En=2.5 MeV, 0+ g.s.
EL.C-S[MB/SR]

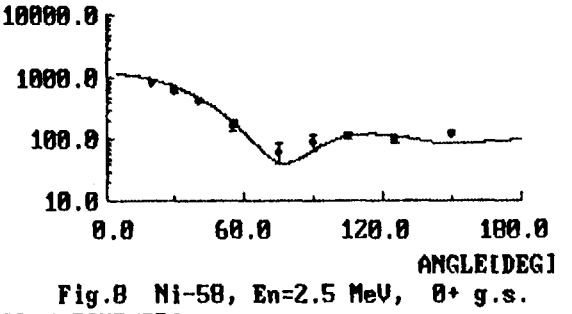

Fig.7 CR-54, En=2.5MeV, 2+(0.835MeV)
INL.C-S[MB/SR]

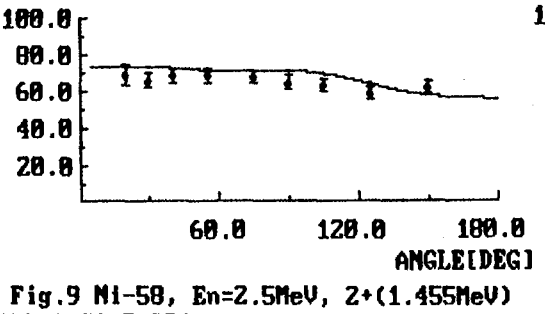

Fig.8 Ni-58, En=2.5 MeV, 0+ g.s.
EL.C-S[MB/SR]

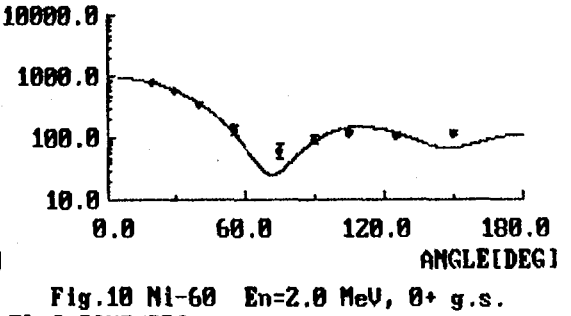

Fig.9 Ni-58, En=2.5MeV, 2+(1.455MeV)
INL.C-S[MB/SR]

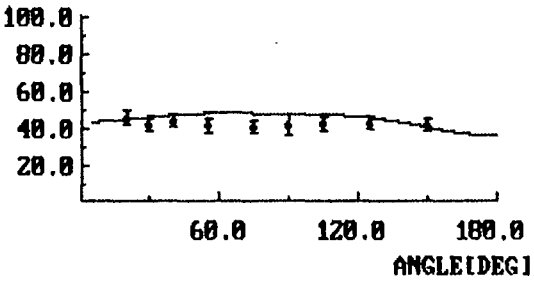

Fig.10 Ni-60 En=2.0 MeV, 0+ g.s.
EL.C-S[MB/SR]

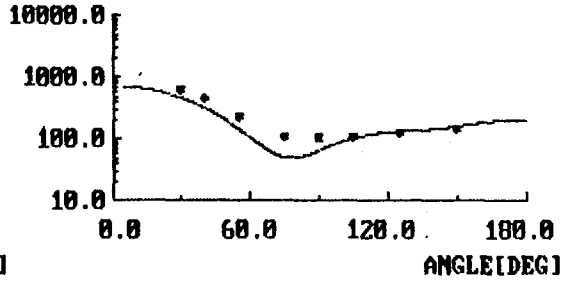

Fig.11 Ni-60, En=2.0MeV, 2+(1.333MeV)

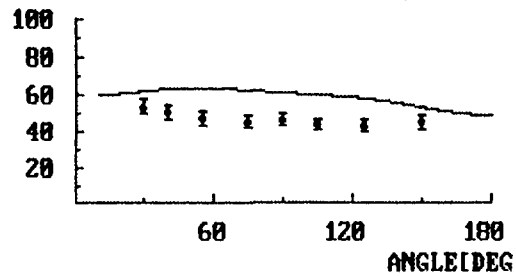

Fig.12 Ni-62 En=2.0 MeV, 0+ g.s.

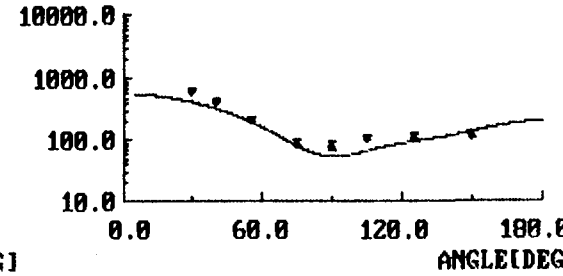

Fig.13 Ni-62, En=2.0MeV, 2+(1.173MeV)

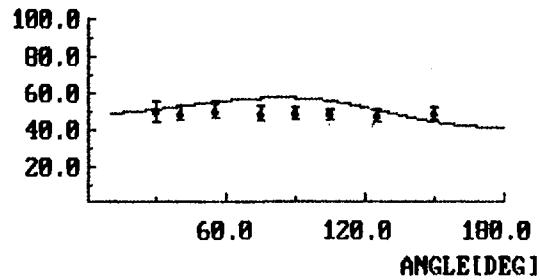

Fig.14 Ni-64 En=3.0 MeV, 0+ g.s.

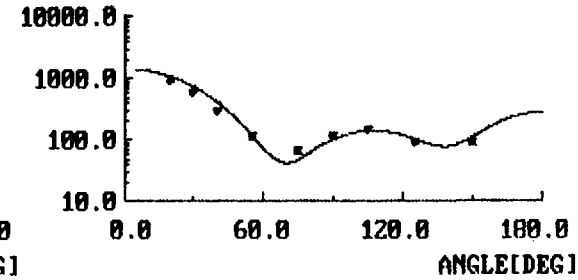

Fig.15 Ni-64, En=3.0MeV, 2+(1.344MeV)

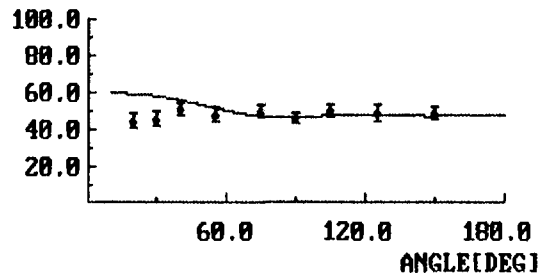

Fig.16 Ni-64, En=3.0MeV, 2+(2.280MeV)

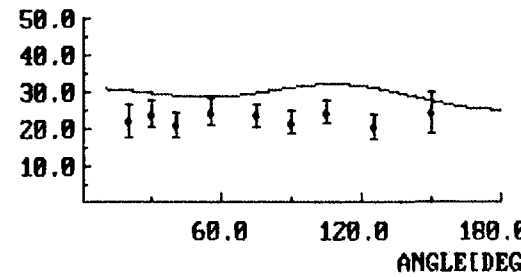

Fig.17 FE-54, En=3.0MeV, 0+ g.s.

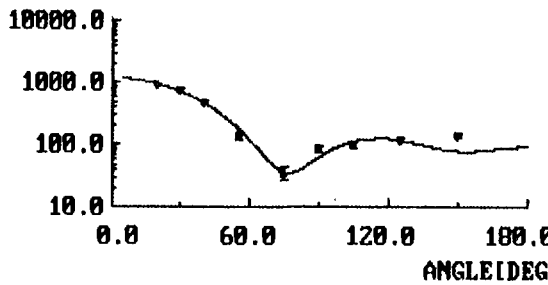

Fig.18 FE-54, En=3.0MeV, 2+(1.408MeV)

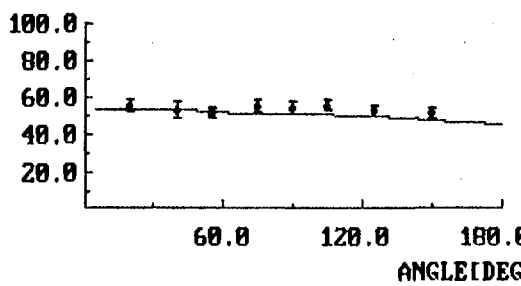

Fig.19 FE-56, En=2.0 MeV, 0+ g.s.

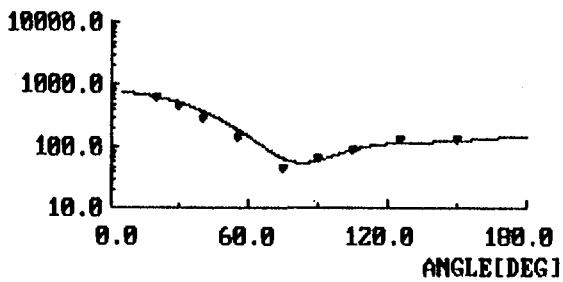

Fig.20 FE-56, En=2.0MeV, 2+(0.847MeV)

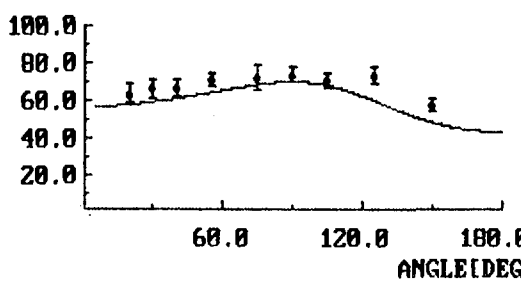

Fig.21 Ti-48, En=2.5 MeV, 0+ g.s.
EL.C-S[MB/SR]

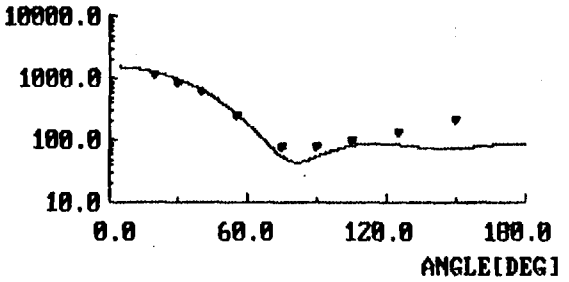

Fig.22 Ti-48, En=2.5MeV, 2+(0.983MeV)
INL.C-S[MB/SR]

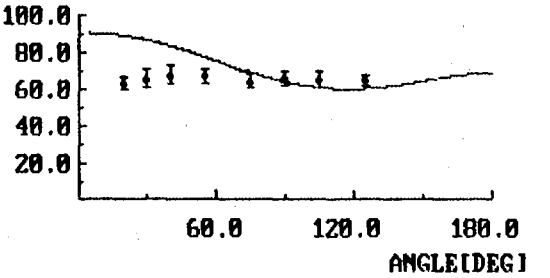

Fig.23 Ni-58, TOTAL CROSS SECTION
TOT.C-S[B]

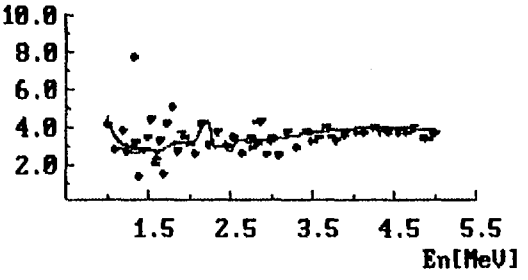

Fig.24 Ni-58, INT. CROSS SEC. 0+ g.s.
INT.C-S[B]

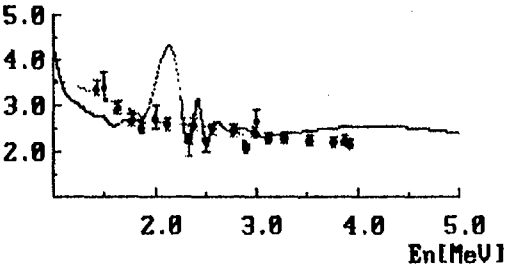

Fig.25 Ni-58,INT. CR. SEC. 2+(1.45MeV)
INT.C-S[MB]

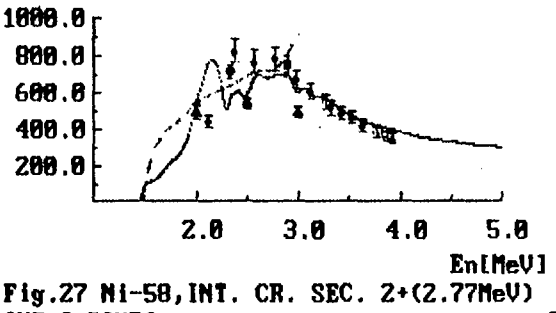

Fig.26 Ni-58,INT. CR. SEC. 4+(2.45MeV)
INT.C-S[MB]

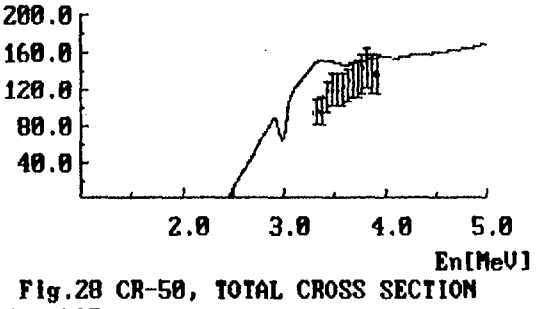

Fig.27 Ni-58,INT. CR. SEC. 2+(2.77MeV)
INT.C-S[MB]

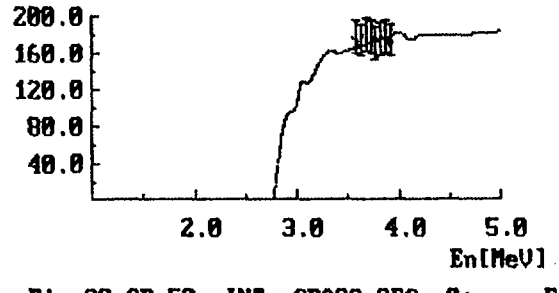

Fig.28 CR-50, TOTAL CROSS SECTION
TOT.C-S[B]

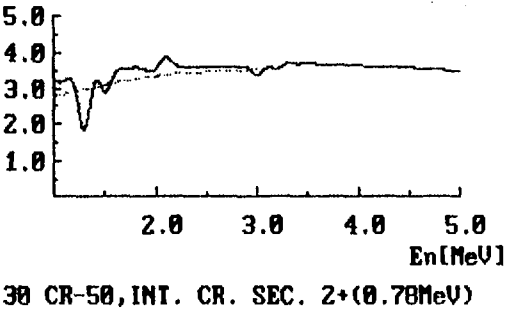

Fig.29 CR-50, INT. CROSS SEC. 0+ g.s
INT.C-S[B]

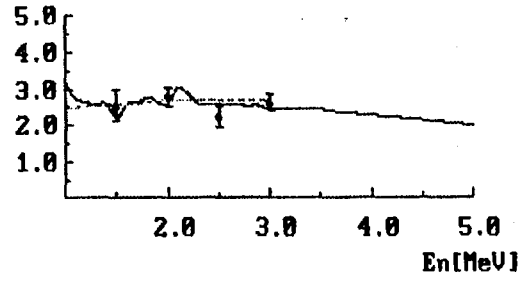

Fig.30 CR-50,INT. CR. SEC. 2+(0.78MeV)
INT.C-S[MB]

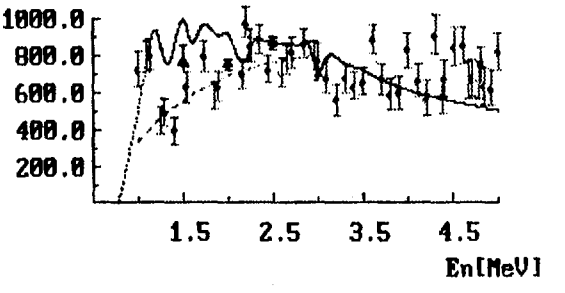

Fig.31 FE-54, TOTAL CROSS SECTION
TOT.C-S[B]

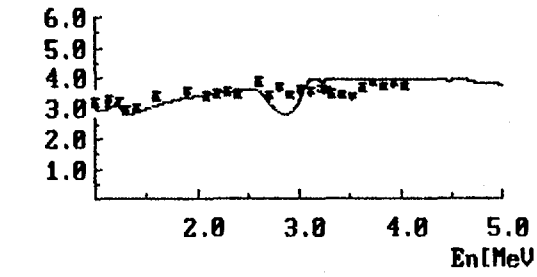

Fig.32 FE-54, INT. CROSS SEC. 0+ g.s.
INT.C-S(B)

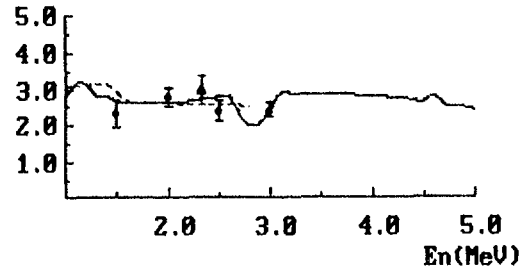

Fig.33 FE-54,INT. CR. SEC. 2+(1.4MeV)
INT.C-S[MB]

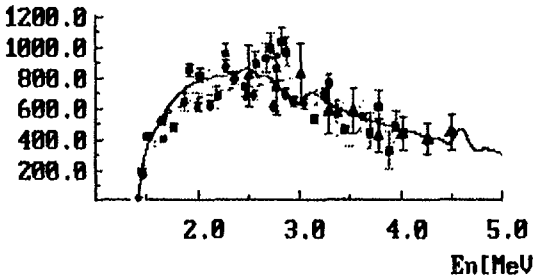

Fig.34 FE-54,INT. CR. SEC. 4+(2.53MeV)
INT.C-S[MB]

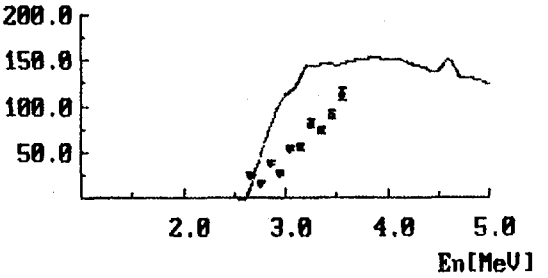

Fig.35 FE-54,INT. CR. SEC. 0+(2.56MeV)
INT.C-S[MB]

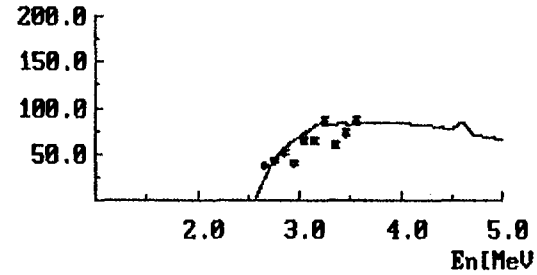

Fig.36 TI-48 TOTAL CROSS SECTION
TOT.C-S[B]

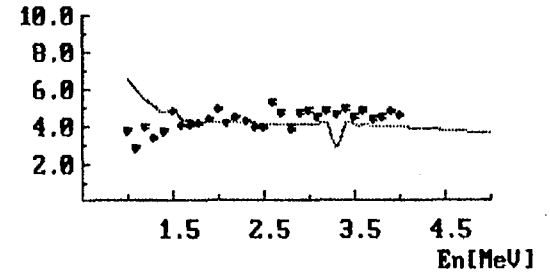

Fig.37 TI-48 INT. CROSS SEC. 0+ g.s.
INT.C-S(B)

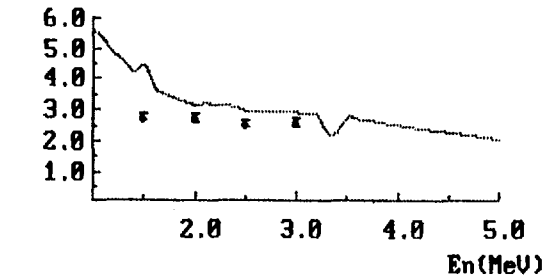

Fig.38 TI-48,INT. CR. SEC. 2+(0.98MeV)
INT.C-S[MB]

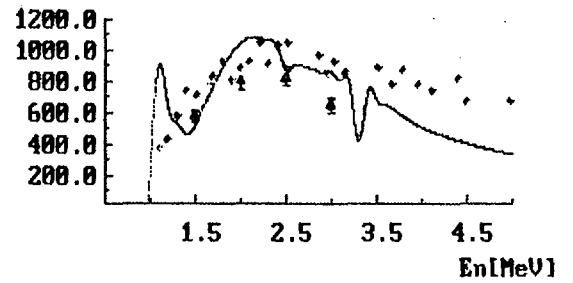

Fig.39 Zn-64, INT. CROSS SEC. 0+ g.s.
INT.C-S[B]

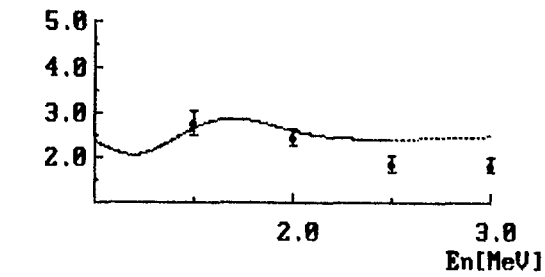

Fig.40 Zn-64,INT. CR. SEC. 2+(0.99MeV)
INT.C-S[MB]

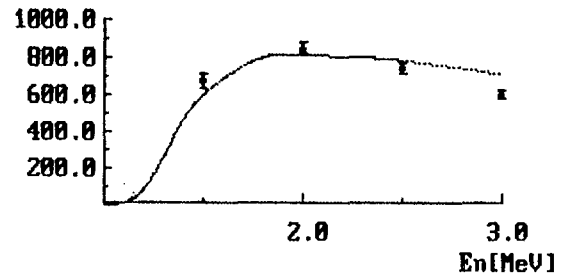

Fig.41 Zn-66, INT. CROSS SEC. 0+ g.s.
INT.C-S[B]

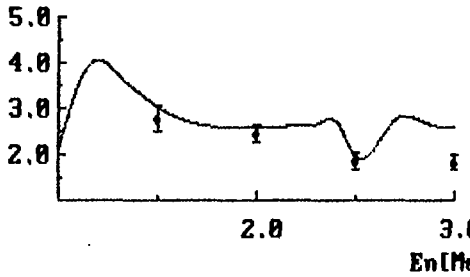

Fig.42 Zn-66,INT. CR. SEC. 2+(1.04MeV)
INT.C-S[MB]

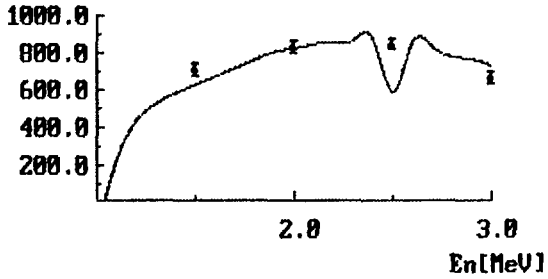

Fig.43 Zn-68, INT. CROSS SEC. 0+ g.s.
INT.C-S[B]

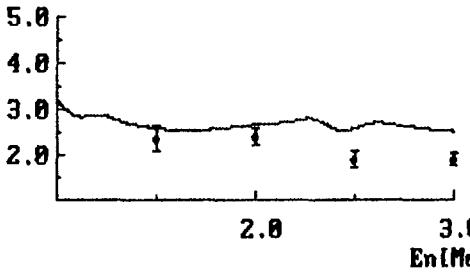

Fig.44 Zn-68,INT. CR. SEC. 2+(1.08MeV)
INT.C-S[MB]